JOURNAL OF OPTOELECTRONICS AND ADVANCED MATERIALS Vol. 9, No. 7, July 2007, p. 2023 - 2029

Recrystallization mechanism of amorphous silicon thin films upon excimer laser crystallization

CHIL-CHYUAN KUO[a,c], WEN-CHANG YEH[b], CHIH-PING HSIAO[a], JENG-YWAN JENG[a]
[a]*Department of Mechanical Engineering, National Taiwan University of Science and Technology No. 43, Keelung Road, Sec. 4, Taipei, Taiwan, 106*
[b]*Department of Electronic Engineering, National Taiwan University of Science and Technology No. 43, Keelung Road, Sec. 4, Taipei, Taiwan, 106*
[c]*Department of Mechanical Engineering, Mingchi University of Technology No. 84 Gungjuan Road, Taishan, Taipei Hsien, Taiwan, 243*

Melting and recrystallization phenomena of plasma-enhanced chemical vapor deposition (PECVD) amorphous silicon (a-Si) thin films for both frontside and backside excimer laser crystallization (ELC) have been investigated by in-situ real-time optical reflectivity and transmissivity (TRORT) measurements with nanosecond time resolution. The longest melt-phase duration of 90-nm-thick a-Si thin films for both frontside and backside ELC is 350 ns. The ablation excimer laser fluence of a-Si thin films for frontside ELC is higher than that of backside ELC because SiO_2 films show anti-reflectivity for excimer laser beam. TRORT measurements reveal that the solidification direction of molten Si for both frontside and backside ELC start from the interface of the sample and the recrystallization mechanism for both frontside and backside ELC are the same.

(Received April 3, 2007, accepted June 27, 2007)

Keywords: Amorphous silicon film, Excimer laser crystallization

1. Introduction

Excimer laser crystallization (ELC) of amorphous silicon (a-Si) is an important technique for fabricating high-quality polycrystalline silicon (poly-Si) films for thin film transistors (TFTs) applications such as active-matrix liquid-crystal displays (AMLCDs) [1].The interest in ELC is mainly due to its cost-effectiveness, since it allows the use of inexpensive glass substrates.

The solid phases of Si are semiconducting but the liquid phase is metallic [2], so that the values of many physical properties such as optical, electrical and thermal constants are very different for the liquid and solid phase at similar temperatures and pressures. Such abrupt discontinuities in physical properties provide unusual and potent opportunities for in-situ real-time optical measurements of the phase transformation of Si thin films. Accordingly, time-resolved optical reflectivity and transmissivity measurements at the film surface have widely been employed to monitor the laser-induced melting and rapid solidification processes in semiconductors. However, the recrystallization mechanisms involved in the process are not understood well even if investigations of ELC of thin a-Si thin films have been widely performed for the past several years, especially for backside ELC.

In this work, a non-invasive in-situ time-resolved optical reflection and transmission (TRORT) [3-4] monitoring system combining two continues-wave He-Ne probe lasers, a digital oscilloscope and three photodiodes is developed to investigate the structural transformation dynamics of PECVD a-Si thin films during ELC. The melt-mediated transformation scenarios of the Si thin films were determined in terms of various excimer laser fluences. After ELC, an extensive microstructural analysis of the resulting poly-Si thin films was performed by Field Emission Scanning Electron (FE-SEM) and high resolution transmission electron microscopy (HR-TEM). According to TRORT, FE-SEM and HR-TEM observations, the recrystallization mechanism of PECVD a-Si thin films is proposed to interpret the formation of grain microstructure and provides a basis for fabrication of single-grain TFTs

2. Experiment

Silane-based a-Si thin films of 90-nm-thick were deposited onto a 0.7-mm-thick glass substrate (Corning 1737) covered with a 300-nm-thick SiO_2 layer by PECVD. These samples were then dehydrogenated by performing a thermal treatment at 500 ℃ for 2 hrs to reduce the content of hydrogen for preventing the ablation caused by sudden hydrogen eruption during ELC. The sample was then held in self-closing tweezers at the end of the cantilever beam fixed on the x-y precision translation stage. The x- and y-axis displacement of the two stages can accurately be controlled (resolution= 0.625 μm) using a LabVIEW^{TM}-based (National Instruments Inc.) custom design interface in order to yield large-area crystallization.

The movement of the focusing lens mounted on the z-axis stage was precisely controlled to adjust the laser energy density during ELC. The pulse excimer energy levels were monitored using pyroelectric Joule meter (Vector H410 SCIENTECH, Inc.). The pulse-to-pulse excimer laser energy variation was found to be less than 5%. All the experiments were carried out under ambient conditions using samples at room temperature.

Figure 1 shows the schematic illustration of experimental setup for monitoring structural transformation dynamics of a-Si thin films during ELC using two probe lasers. Figure 2 shows the experimental configurations of both backside ELC and frontside ELC used for measuring the time evolution of the frontside reflectivity (FSR), frontside transmissivity (FST) and backside reflectivity (BSR). The utilization of the three configurations provides complementary information of surface and interface between film and glass substrate during ELC. The XeF excimer laser can pass through the glass substrate because the wavelength of the XeF excimer laser is attributed to near ultraviolet. Accordingly, the backside ELC can be employed in this study. The a-Si thin films were irradiated by a XeF excimer laser operating at a wavelength of 351nm with a short pulse of 25 ns in full-width-half-maximum. The repetition rate was kept at 1 Hz to avoid cumulative heating of the samples. The sample was moved to a new position after each ELC by manipulating the self-developed man-machined interface. A stainless slit (2 mm×15 mm) is employed to transform the incident Gaussian beam into a rectangular beam spot with energy variation within ±10 %. During ELC, in-situ real-time TRORT measurements were performed using two continuous wave He-Ne probe lasers operating at a wavelength of 632.8 nm. A pinhole with a diameter of 0.3mm was mounted in front of the He-Ne probe laser to increase the resolution of TRORT measurements. He-Ne laser had a 45° of incidence from the normal of the sample's surface and focused on the center of the laser-irradiated spot. The reflected beam from the sample was focused on the photodiode (fast Si PIN). The interference filter was mounted in front of the photodiode, allowing only red light from the He-Ne probe laser to contribute to the detected signal. The photodiode is placed in an excellent position where the maximum signal is obtained during ELC. A quartz beam splitter was employed to reflect 10 % of the excimer laser beam to a triggering photodiode for triggering the record of reflection spectra using a fast digital storage oscilloscope (LeCroy WS454, bandwidth =500 MHz, sample rate= 2GHz/s).The response time of the entire TRORT measurement is 1ns. The melt-mediated transformation scenarios, melt-phase duration of molten Si, surface melting threshold, complete melting excimer laser fluence and Si film ablation threshold were investigated by the TRORT measurements during ELC. After ELC, an extensive microstructural analysis of the resulting poly-Si thin films were performed using FE-SEM (JEOL JSM-6500F) operated at an acceleration voltage of 15 kV(resolution ~1.5 nm)and HR-TEM (JEOL JEM-2010) operated at an acceleration voltage of 300 kV(resolution ~0.2 nm). Before FE-SEM observation, the crystallized silicon films were Secco-etched (50% HF: H_2O: CrO_3=200 cc: 100 cc: 1.5g) for 3s in order to highlight the grain boundaries and intra-grain defects.

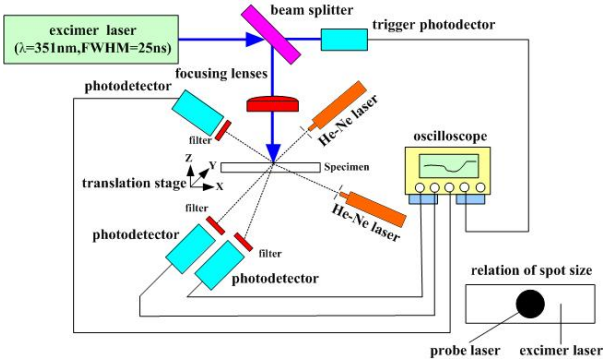

Fig. 1. Schematic illustration of experimental setup for monitoring structural transformation dynamics of a-Si thin films during ELC using two probe lasers. The relation between probe laser spot size and excimer laser spot size is shown on the right-hand side below.

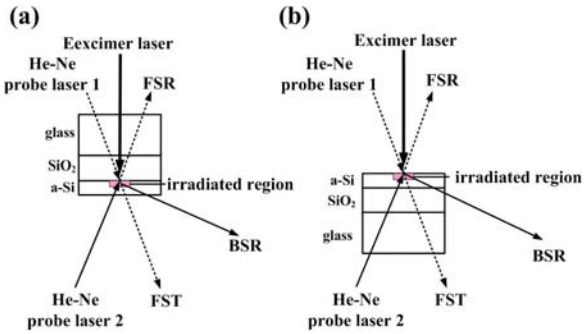

Fig. 2. Experimental configurations of (a) backside ELC and (b) frontside ELC used for measuring the time evolution of the FSR, FST and BSR.

3. Results and discussion

Fig. 3 shows cross-sectional bright field TEM images of excimer laser crystallized Si thin films at various energy densities. Following ELC at laser energy density range from 90 mJ/cm^2 to 700 mJ/cm^2, the experimental results can be divided into five distinct regimes according to different laser energy densities: heating of Si films [Figure 3(a)], partial melting [Figure 3(b)], near-complete melting [Figure 3(c)], complete melting [Figure 3(d)], and ablation of Si films. At a laser energy density of 60 mJ/cm^2, the reflection and transmission signals exhibited an abrupt

drop, followed by a relaxation to the initial value indicating that the a-Si thin films did not melt but were merely undergoing heating and cooling during ELC. The changes in the TRORT signals were significantly governed by the increase in the extinction coefficient and the temperature-dependent optical constants of Si thin films [5]. This is also confirmed by the corresponding SEM images because no polycrystalline silicon (poly-Si) grains were observed in the sample. As the excimer laser fluence is increased above the surface melting threshold of a-Si thin films, two distinct phase transformation sequences take place during ELC. One is the melting of a-Si thin films following the absorption of laser energy and the other is the nucleation and subsequent growth of poly-Si grains as the sample cools. The formation of nuclei is a crucial step for the phase transition. Figure 4 shows the clear evidence of melting and resolidification sequence during ELC at excimer laser fluence of 150 mJ/cm^2 .The data are normalized to the initial reflectivity and transmissivity of a-Si thin films. The sample initially absorbs the excimer laser fluence (from point A to B) and then melts. The reflection signal increases because the reflectivity of Si thin films changes from 32 % to 76 % upon melting during the phase transition from solid to liquid, which exhibits the metallic behavior [6]. The significant decrease in the transmission signal is caused by crystallization of the molten Si. A plateau (from point B to C) in the reflection signal is observed because the melt depth of molten Si is more than double the penetration depth of He-Ne probe laser [7].Between points C and D, the reflectivity decreases, indicating the solidification process. The melt-phase duration defined by Auston et al. [8] is indicated at the interval between points B and E. Fig. 5 shows melt-phase duration as a function of laser fluence for both frontside and backside ELC. The melt-phase duration increases with increasing excimer laser fluence for both frontside and backside ELC. The longest melt-phase duration of 90-nm-thick a-Si thin films for both frontside and backside ELC is 350 ns. This result reveals that the thickness of a-Si thin films is the key factor affecting the melt-phase duration during ELC rather than the approaches of ELC. Fig. 6 shows that the ablation excimer laser fluence (Eab) and complete melting laser fluence (Ec) of a-Si thin films for frontside ELC is higher than that of backside ELC, while the surface melting threshold of a-Si thin film for frontside and backside ELC are the same. These effects are mainly attributed to the anti-reflectivity characteristic of SiO_2 films for excimer laser beam [9]. For a-Si thin films of the same thickness, the lower excimer laser fluences for complete melting and ablation of Si thin films are needed by backside ELC when compared with frontside ELC. Consequently, backside ELC approach is a good candidate for laser crystallization in terms of energy-saving of excimer laser.

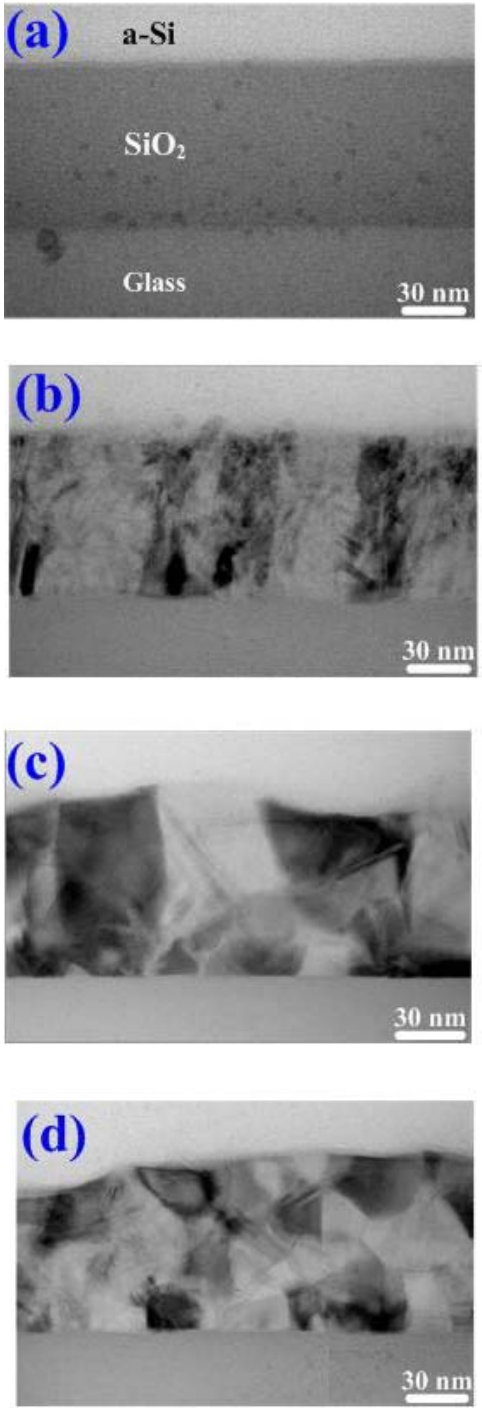

Fig. 3. Cross-sectional bright field TEM images of excimer laser crystallized Si thin films at various energy densities. (a) E=60 mJ/cm^2.The Si thin films remain amorphous structure. (b)E=100 mJ/cm^2. The Si thin films have completely converted into poly-Si due to explosive crystallization. (c)E=350 mJ/cm^2.Large-grained poly-Si are formed due to SLG mechanism. (d) E=500 mJ/cm^2. Fine-grained poly-Si are formed due to homogeneous random nucleation.

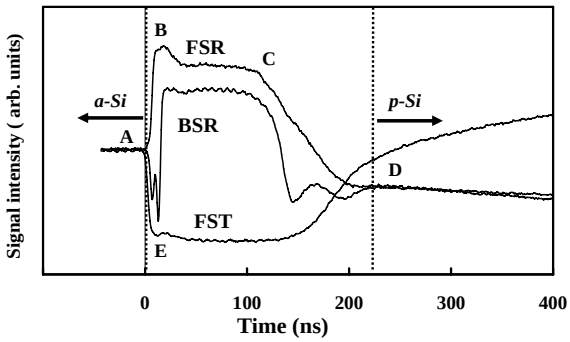

Fig. 4. Typical signals of FSR, FST and BSR recorded by digital oscilloscope, identifying the melting and resolidification sequence during ELC at excimer laser fluence of 150 mJ/cm^2.

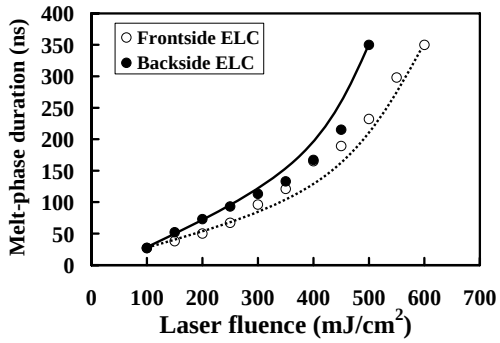

Fig. 5. Melt-phase duration as a function of laser fluence for both frontside and backside ELC.

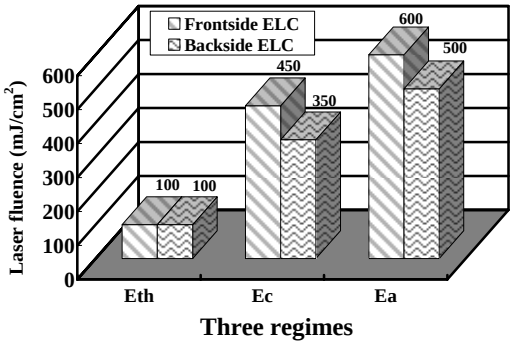

Fig. 6. Surface melting threshold, complete melting excimer laser fluence and ablation excimer laser fluence of a-Si thin films for both frontside and backside ELC.

Fig. 7 shows the surface reflectivity, interface reflectivity and transmissivity of the sample during ELC as a function of time at complete melting regime for both frontside and backside ELC. The most striking feature in this figure is the faster resolidification velocity of the surface (line L1) than that of the interface (line L2) of the silicon film, revealing that the solidification direction of molten Si for both frontside and backside ELC can be deduced from the interface toward the surface, as shown in Figure 8. The occurrence of recalescence after solidification is clearly observed at the interface of the sample, illustrated at the second maximum of BSR signal of frontside ELC and FSR signal of backside ELC, respectively. The massive release of solidification heat causes the reheating and partial remelting of a-Si thin films after its complete solidification. This result is in good agreement with the observation of amorphous germanium (a-Ge) under picosecond laser irradiation [10].

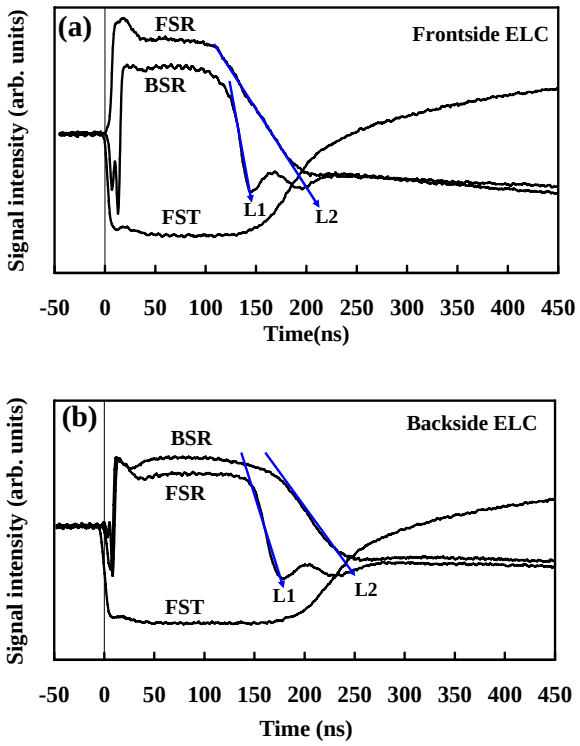

Fig. 7. Surface reflectivity, interface reflectivity and transmissivity of the sample during ELC as a function of time at complete melting regime for both (a) frontside ELC and (b) backside ELC.

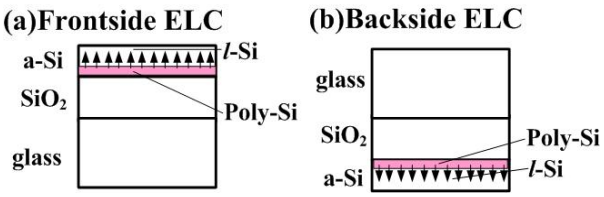

Fig. 8. Solidification direction of Si thin films for (a) frontside ELC and (b) backside ELC.

Fig. 9 shows the SEM images of the Secco-etched poly-Si films in different regimes. The amorphous regions

of the silicon thin films have been etched away, leaving only poly-Si on glass substrate. In the partial melting regime, there is an increase in grain size with increase in excimer laser fluence. The grain size, however, reaches the maximum because of super lateral growth (SLG) nucleation in the near-complete melting regime. It is remarkable that the maximum size of the average grain reaches 1 μm in the SLG regime because the lateral growth results from explosive crystallization [11] combined with liquid phase growth. Indeed, this scenario was significantly supported by the observation of Aichmayr et al. [12]. In the complete melting regime, fine-grained poly-Si is observed due to homogeneous random nucleation .When the laser fluence exceeds the ablation excimer laser fluence, some a-Si thin films will evaporate, resulting in poor morphology of the sample. As expected, the measurements show that the dependence of grain size of PECVD a-Si thin films on the crystallization excimer energy densities exhibits characteristics similar to reports on LPCVD a-Si thin films [13], with two distinct regimes (the low energy density and high energy density regimes) clearly discernable. In the low energy density regime, grain sizes slowly increase because the melt depth increases with increasing excimer laser energy density. On the other hand, in the high energy density regime, grain size is not affected by variations in excimer laser fluence since the recrystallization mechanism is changed [14]. Fig. 10 shows the solidification directions of molten Si starting from the boundary between the irradiated area and a-Si thin films after a complete melting excimer laser irradiation because the excimer laser spot is surrounded by a-Si thin films.

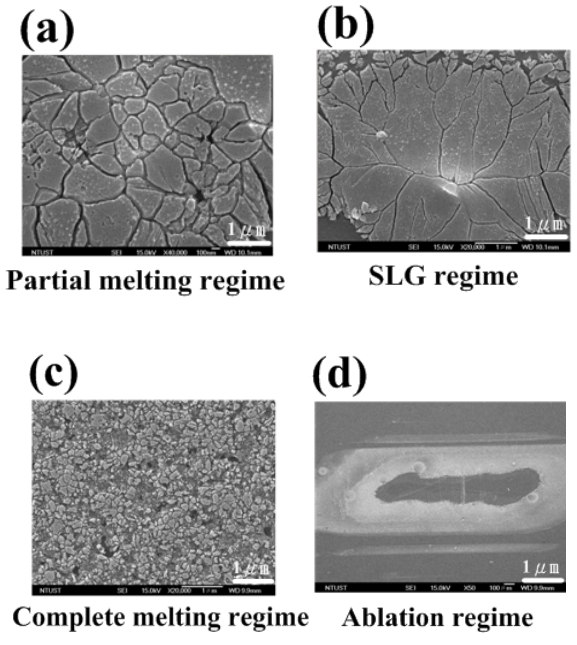

Fig. 9. FE-SEM images of the Secco-etched poly-Si films in different regimes.

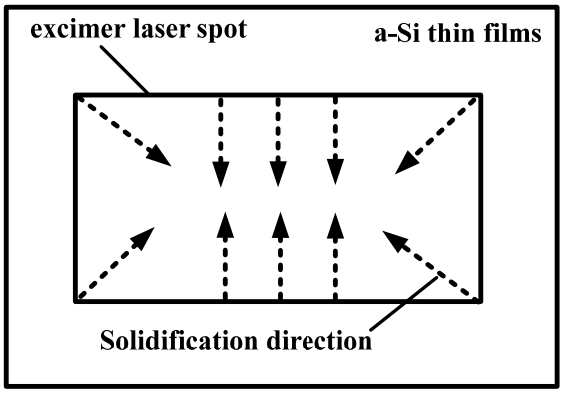

Fig. 10. Schematic illustration of solidification direction of molten Si.

According to both TRORT investigations and FE-SEM observations, the recrystallization mechanisms for both frontside and backside ELC upon ELC are the same as summarized in Figure 11, revealing the formation of grain microstructure for three distinct regimes. The recrystallization mechanisms can be divided into three regimes, depending on different excimer laser fluences illustrated in Figure 6. Owing to a XeF excimer laser pulse inherent with Gaussian beam profile, the molten Si has a steep lateral temperature gradient; the higher temperature within the center molten zone results in a correspondingly longer time to reach the deep supercooling regime where spontaneous nucleation occurs. The excimer laser beams were focused through a signal cylindrical plano-convex lens, resulting in larger lateral temperature gradient in the direction of the two axes of the irradiated rectangular spots. Thus, the crystal growth propagated from outside to the center of the irradiated spots.

The complete melting regime describes the situation that is encountered when the incident excimer laser fluence is sufficiently high to complete melting of the Si thin films. Owing to the amorphous structure of SiO_2, epitaxial regrowth from the surface of the glass substrate is not possible. In the complete melting regime, the recrystallization mechanism is significantly governed by homogeneous nucleation in a deeply supercooled melt, leading to small (smaller than 100 nm),globular grains randomly distributed throughout the Si thin films [15].

The partial melting regime describes the situation that is encountered when the incident excimer laser fluence is sufficient to induce melting of a-Si thin films, but is low enough such that a continuous layer of solid Si remains at the maximum extent of primary melting. In the partial melting regime, the maximum temperature remains close to the melting point of a-Si tin films and the grain size gradually increases from a few tens up to several hundreds of nanometers, depending on different excimer laser fluences.

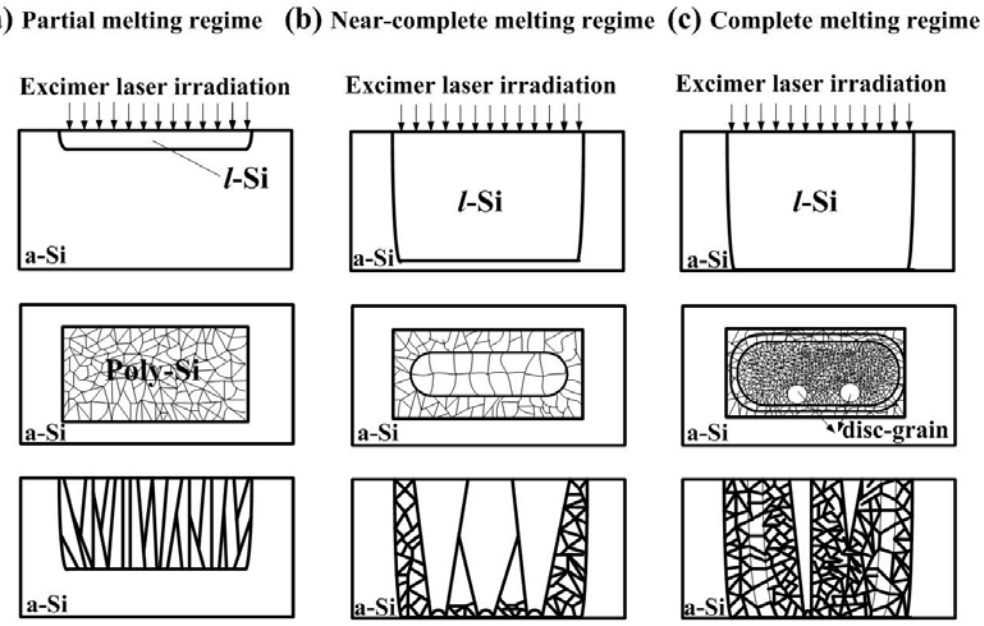

Fig. 11. Recrystallization mechanisms of Si thin films for three distinct regimes upon ELC.

Between the partial and complete melting regime, a SLG regime was identified to occur within a narrow process window at the transition between the two distinct regimes. In the near-complete melting regime, the large-grained poly-Si can be obtained. Im et al. [16] have explained the SLG phenomenon, which is a regrowth process commencing from the residual un-melted Si islands in a liquid matrix. The fewer the Si islands that remain, the larger their separation will be. Consequently, the longer they can grow laterally. The maximum attainable grain size is determined by the onset of copious nucleation in the continuously cooling liquid ahead of the crystallization interface. A SLG region can still be observed in the complete melting regime, but the region is very narrow because the excimer beam is a Gaussian profile and the molten Si cools very rapidly [17].Among the three distinct regimes, the SLG regime is essential for fabrication of single-grain TFTs by backside ELC with a special sample structure named photosensitive capping layer [18].The range of excimer laser fluence for achieving large-grained poly-Si is defined as the process window. The process window of total excimer energy density is not sufficiently wide in comparison with the pulse-to-pulse fluctuation of a modern commercial excimer laser machine. In general, the energy density of SLG has a very narrow process window, typically about 1.5% [19] and 2.5 % [20].The process window has been experimentally observed to reach 5 % by TRORT measurements in our previous investigation [21]. These results demonstrate that this recrystallization mechanism of a-Si thin films is sufficient for fabricating single-grain TFTs by backside ELC, which are essential for the device-to-device uniformity of high-performance TFTs.

4. Conclusions

Recrystallization mechanisms of PECVD a-Si thin films upon excimer laser crystallization have been experimentally investigated to interpret the formation of the grain microstructure for both frontside and backside ELC by a comprehensive SEM, cross-sectional TEM and TRORT analysis. The recrystallization mechanisms for both frontside and backside ELC are the same and the recrystallization mechanism of PECVD a-Si thin films sensitively depends on the irradiated excimer laser fluence, which controls the thickness of the molten Si layer and the melt-phase duration. Backside ELC approach is a good candidate for laser crystallization in terms of energy-saving of excimer laser. This result provides a basis for fabrication of single-grain TFTs under appropriate conditions by backside ELC, which are essential for the device-to-device uniformity of high-performance TFTs.

References

[1] Y. F. Chong, K. L. Pey, A. T. S. Wee, M. O. Thompson, C. H. Tung, A. See, Appl. Phys. Lett. **81**, 3786 (2002).
[2] G. E. Jellison, Jr., D.H. Lowndes, Appl. Phys. Lett. **47**, 718 (1985).
[3] C. C. Kuo, W. C. Yeh, C. B. Chen, J. Y. Jeng, Thin Solid Films **515**, 1651 (2006).
[4] C. C. Kuo, W. C. Yeh, C. B. Chen, J. Y. Jeng, Mat. Sci. Forum **505**, 337 (2006).
[5] G. E. Jellison, Jr., D. H. Lowndes, J. Appl. Phys. **60**, 841 (1986).

[6] D. von der Linde, N. Fabricius, Appl. Phys. Lett. **41**, 991 (1982).
[7] J. Boneberg, P. Leiderer, Phys. Stat. Sol **166**, 643 (1998).
[8] D. H. Auston, C. M. Surko, T. N. C. Venkatesan, R. E. Slusher, J. A. Golovchenko, Appl. Phys. Lett. **33**, 43 (1978)
[9] H. J. Kim, J. S. Im, Appl. Phys. Lett. **68**, 1513 (1996).
[10] J. Siegel, J. Solis, C. N. Afonso, Appl. Phys. Lett. **75**, 1071 (1999).
[11] M. O. Thompson, G. J. Galvin, J. W. Mayer, Phys. Rev. Lett. **52**, 2360 (1984).
[12] G. Aichmayr, D. Toet, M. Mulato, P. V. Santos, A. Spangenberg, R. B. Bergmann, J. Non-Cryst. Solids **227**, 921 (1998).
[13] J. S. Im, H. J. Kim, M. O. Thompson, Appl. Phys. Lett. **63**, 1969 (1993).
[14] J. P. Leonard, J. S. Im, Appl. Phys. Lett. **78**, 3454 (2001).
[15] S. R. Stiffler, M. O. Thompson, P. S. Peercy, Phys. Rev. B **43**, 9851 (1991).
[16] J. S. Im and H. J. Kim, Appl. Phys. Lett. **64**, 2303 (1994).
[17] M. Hatano, S. Moon, M. Lee, K. Suzuki, C. P. Grigoropoulos, J. Non-Cryst. Solids **266**, 654 (2000).
[18] W. C. Yeh and M. Matsumura, Jpn. J. Appl. Phys. **41**, 1909 (2002).
[19] R. Ishihara, A. Burtsev, and P.F.A. Alkemade, Jpn. J. Appl. Phys. **39**, 3872 (2000).
[20] D. Pribat, P. Legagneux, C. Collet, F. Plais, O. Huet, C. Reita, Proceedings of the Active-Matrix Liquid-Crystal Displays (AM-LCD), Tokyo, Japan, July 9-10, 1999, p.9.
[21] C. C. Kuo, W. C. Yeh, C. B. Chen, J. Y. Jeng, Proceedings of 2005 IEEE/ASME International Conference on Advanced Manufacture, Taipei, Taiwan R. O. C., November 28-December 2, 2005, p.337.

*Corresponding author: jacksonk@ns1-mit.edu.tw